

Article

Methanation of CO₂ Using MIL-53-Based Catalysts: Ni/MIL-53–Al₂O₃ versus Ni/MIL-53

Oana Grad, Gabriela Blanita , Mihaela D. Lazar and Maria Mihet *

National Institute for Research & Development of Isotopic and Molecular Technologies—INCDTIM, 67-103 Donat Str., 400293 Cluj-Napoca, Romania; oana.grad@itim-cj.ro (O.G.); gabriela.blanita@itim-cj.ro (G.B.); diana.lazar@itim-cj.ro (M.D.L.)

* Correspondence: maria.mihet@itim-cj.ro; Tel.: +40-264-584037

Abstract: MIL-53 and the MIL-53–Al₂O₃ composite synthesized by a solvothermal procedure, with water as the only solvent besides CrCl₃ and benzene-1,4-dicarboxylic acid (BDC), were used as catalytic supports to obtain the novel MIL-53-based catalysts Ni(10 wt.)/MIL-53 and Ni(10 wt.)/MIL-53–Al₂O₃. Ni nanoparticle deposition by an adapted double-solvent method leads to the uniform distribution of metallic particles, both smaller (≤ 10 nm) and larger ones (10–30 nm). MIL-53–Al₂O₃ and Ni/MIL-53–Al₂O₃ show superior thermal stability to MIL-53 and Ni/MIL-53, while MIL-53–Al₂O₃ samples combine the features of both MIL-53 and alumina in terms of porosity. The investigation of temperature's effect on the catalytic performance in the methanation process (CO₂:H₂ = 1:5.2, GHSV = 4650 h^{−1}) revealed that Ni/MIL-53 is more active at temperatures below 300 °C, and Ni/MIL-53–Al₂O₃ above 300 °C. Both catalysts show maximum CO₂ conversion at 350 °C: 75.5% for Ni/MIL-53 (methane selectivity of 93%) and 88.8% for Ni/MIL-53–Al₂O₃ (methane selectivity of 98%). Stability tests performed at 280 °C prove that Ni/MIL-53–Al₂O₃ is a possible candidate for the CO₂ methanation process due to its high CO₂ conversion and CH₄ selectivity, corroborated by the preservation of the structure and crystallinity of MIL-53 after prolonged exposure in the reaction medium.



Citation: Grad, O.; Blanita, G.; Lazar, M.D.; Mihet, M. Methanation of CO₂ Using MIL-53-Based Catalysts: Ni/MIL-53–Al₂O₃ versus Ni/MIL-53. *Catalysts* **2021**, *11*, 1412. <https://doi.org/10.3390/catal11111412>

Academic Editor: Wojciech Gac

Received: 13 October 2021

Accepted: 19 November 2021

Published: 21 November 2021

Publisher's Note: MDPI stays neutral with regard to jurisdictional claims in published maps and institutional affiliations.



Copyright: © 2021 by the authors. Licensee MDPI, Basel, Switzerland. This article is an open access article distributed under the terms and conditions of the Creative Commons Attribution (CC BY) license (<https://creativecommons.org/licenses/by/4.0/>).

Keywords: MIL-53–Al₂O₃; Ni/MIL-53 catalyst; Ni/MIL-53–Al₂O₃ catalyst; methanation of CO₂

1. Introduction

Lately, the methanation of CO₂ has experienced a revived interest due to the fact that it might meet two challenges simultaneously: (1) electrical *energy storage* in the form of methane by the use of hydrogen produced using renewable energy [1–3] (the Power-to-Gas concept); and (2) *abatement of CO₂ emissions* by the utilization of CO₂ (the carbon capture and utilization concept, CCU), rather than CO₂ capture and storage (CCS) [4–6]. Although theoretically very attractive, one of the major problems of CO₂ methanation is the catalytic process, which needs efficient catalysts in order to activate the very stable CO₂ molecule and to overcome the kinetic limitations given by the eight-electron process involved for the complete reduction from CO₂ to CH₄ [5].

Generally, catalysts of the metal/support type were used in the methanation of CO₂, with various combinations between selected metals (i.e., Ni, Ru, Rh, Pt, Pd, Fe, Co) [7–10] or supports (i.e., Al₂O₃, SiO₂, ZrO₂, TiO₂, CeO₂, MCM-41, UiO-66, MIL-101, MOF-5, Al₂O₃–MIL-53, etc.) [9–12]. However, Ni/Al₂O₃ is one of the most widely used catalysts due to its good catalytic activity and its economic advantage [8,13,14]. Several approaches were considered to improve the catalytic performance of Ni-based catalysts, among which promotion with noble metals to enhance the activation of hydrogen [8,14,15] or the addition of basic oxides to enhance the activation of the acidic CO₂ molecule [16–19] were considered. Another interesting approach is to simultaneously pursue the enhancement of both H₂ and CO₂ activation by the use of supports with very large surface areas (i.e., ≥ 250 m²/g), which could ensure an increased metal dispersion necessary for the activation of H₂ [20], as well

as an increased number of CO₂ activation sites due to the large surface area [21–23]. For this goal, metal–organic frameworks (MOFs) were spotted on the large scene of materials owing to their special properties given by their large surface area and uniform porosity, structural diversity, tailorability, and good gas sorption capacities [23–26]. There are only a few reports on the use of MOF-based catalysts in the methanation of CO₂: Ni@MOF-5 [27], Ni@MIL-101 [22,28], Ni@UiO-66 [28,29], or Pt/UiO-66 [30], although MOFs, MOF composites, or MOF derivatives have found their way for diverse energy applications [23,31]. However, MOFs' low density as a consequence of their large porosity gives them low mechanical and thermal stability [32,33], which makes them less attractive for catalytic applications, despite their exceptional properties. Thus, the shaping of MOFs either by compacting the powders by pressing [25,32,34] or immobilization into or onto different structures [33,35–37] becomes of utmost importance. If the compaction of powders by pressing leads to a decrease in surface area due to the alteration of the crystalline structure [25], or to the amorphization of the MOF depending on the applied pressure [32], the immobilization of MOFs onto different structures is not only an elegant shaping approach, but could bring important advantages, as diffusion limitations given by the narrow pores of the MOF might be surpassed due to the meso-microporous nature of the MOF composite thus obtained [25,37,38]. Up to now, different MOFs have been immobilized on either silica (MOF-5@SiO₂ [39,40], MOF-5@SBA-15 [41], HKUST-1@MCM-41 [42], HKUST-1@SiO₂ [43]) or alumina supports (HKUST-1@boehmite [38], ZIF-8@Al₂O₃ [37], MOF-5@ α -Al₂O₃ [44], MIL-101@ α -Al₂O₃ [35]) using different synthetic approaches.

Following our experience in the methanation of CO₂, either on alumina-supported Ni catalysts [15] or on MOF-based catalysts [28,30], we aimed to shape MOFs in order to obtain more stable MOF-based catalytic supports [45]. Thus, in our quest for shaping MOFs by crystallization on preformed structures, MIL-101 was first chosen to be immobilized on alumina pellets due to its large surface area and its interesting mesoporous structure given by the two types of cavities (2.9 and 3.4 nm), which can be accessed through apertures of 1.2 and 1.6 nm width [46]. Thus, starting from the synthesis conditions for MIL-101 and pursuing the synthesis of the MIL-101–Al₂O₃ composite, it was initially found that MIL-53 was also immobilized on the selected amount of alumina, besides the targeted MIL-101. MIL-53 and MIL-101 are two members of the chromium benzenedicarboxylate family of MOFs (Cr-BDCs), with different porosity characteristics: MIL-101 possesses BET surface areas >3000 m²/g and a large pore volume due to its special mesoporous structure, while MIL-53 gives surface areas up to 1500 m²/g and a lower pore volume of 0.6 cm³/g due to its microporous structure (pores around 0.85 nm) [47]. On the other hand, MIL-53 is a three-dimensional framework with a one-dimensional pore channel system, and exhibits a very interesting breathing effect given by its three forms: the pores of the as-synthesized MIL-53 (MIL-53as) filled with disordered benzene-1,4-dicarboxylic acid (BDC) can be liberated by calcination to give the high-temperature MIL-53 structure (MIL-53ht), which by hydration at room temperature gives the low-temperature form (MIL-53lt) [47].

If MIL-101 and more so the composite material MIL-101–Al₂O₃, obtained by immobilization on alumina, proved their efficiency as catalytic supports in the methanation of CO₂ [28,45], what is the case for their MIL-53 homologues? Since MIL-53 is known for its CO₂ adsorption capacity even in its hydrated form [48,49], and considering that it is generally accepted that the support plays an important role in the activation and dissociation of CO₂ during the methanation process [8], MIL-53-based catalytic supports could be an interesting choice for this reaction. Therefore, the aim of this work is to report for the first time the synthesis of MIL-53-coated alumina, giving the MIL-53–Al₂O₃ composite, and to evaluate its performance as a catalytic support in the methanation of CO₂. Therefore, a Ni(10 wt.)/MIL-53–Al₂O₃ catalyst synthesized by an adapted double-solvent method was tested in the CO₂ methanation process and compared to its homologue Ni(10 wt.)/MIL-53. It should be highlighted that both MIL-53 and the MIL-53–Al₂O₃ composite were obtained under hydrothermal conditions, with no added HF, after only 12 h reaction time, as compared to 72 h for the classical synthesis procedure for MIL-53 [47], a

less time- and energy-consuming synthetic approach, and therefore more advantageous from the environmental point of view.

2. Results and Discussion

2.1. Structural Characteristics of Catalysts

As previously reported, in the attempt of immobilizing MIL-101 on alumina particles starting from the synthesis procedure of MIL-101, it was noticed that the equimolar mixture of BDC and CrCl_3 (220 °C, 24 h) results in a mixture of both MIL-101 and MIL-53 covering the alumina particles introduced in the reaction pot [45]. Thus, the synthesis procedure was modified with the goal to obtain either MIL-101 or MIL-53 on the alumina particles, giving MIL-101- Al_2O_3 [45] and MIL-53- Al_2O_3 composites, respectively. The MIL-53- Al_2O_3 composite was obtained successfully after one deposition procedure at 150 °C, 12 h.

Comparative analysis of XRD patterns for MIL-53 and the MIL-53- Al_2O_3 composite (low-temperature forms) (Figure 1) reveals that characteristic peaks of MIL-53 are well defined in both samples, indicating that MIL-53 was successfully obtained either alone or deposited on the alumina particles. The only notable difference between the synthesized MIL-53 and MIL-53- Al_2O_3 is that the diffraction peak situated at 12° in the case of MIL-53 is slightly shifted to the right in the case of MIL-53- Al_2O_3 . Besides the diffraction lines corresponding to the deposited MOF, the XRD pattern of the MIL-53- Al_2O_3 composite also show a characteristic reflexion corresponding to γ -alumina situated at 67.1° (JCPDS card no. 50-0741) (inset of Figure 1). Following the deposition of Ni nanoparticles by the double-solvent method, both MIL-53 and MIL-53- Al_2O_3 supports preserve their structure, the characteristic diffraction lines of MIL-53 being evident in both Ni/MIL-53 and Ni/MIL-53- Al_2O_3 samples (Figure 1). Characteristic diffraction lines for Ni are slightly noticeable only at 44.5° corresponding to Ni (1 1 1) (JCPDS card no. 65-0380), suggesting the formation of small and well dispersed Ni nanoparticles on either MIL-53 or MIL-53- Al_2O_3 supports (see inset of Figure 1). This observation is in agreement with previous reports related to the encapsulation of metal nanoparticles inside the pores of different MOFs or MOF-based composites: Pd(5 wt.)/MIL-101 [50], Ni(10 wt.)/MIL-101 [28,45], Ni(20 wt.)/UiO-66 [29], or Ni(10 wt.)/MIL-101- Al_2O_3 [45].

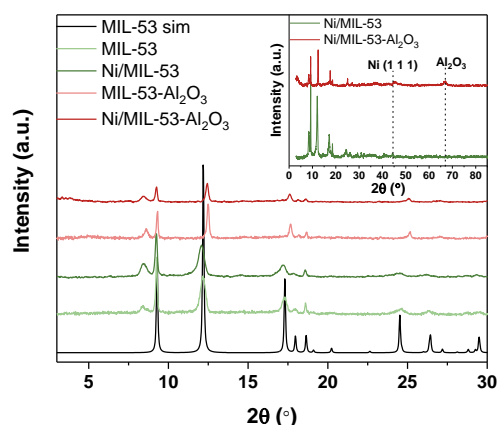


Figure 1. Low-angle XRD patterns of MIL-53 and MIL-53- Al_2O_3 samples, and XRD patterns of the corresponding Ni-based catalysts (Ni/MIL-53, Ni/MIL-53- Al_2O_3)—inset.

Nitrogen adsorption–desorption isotherms of the MIL-53-based samples, as well as their pore size distribution, are presented in Figure 2, while corresponding surface area values, total pore volumes, micropore volumes, and average pore dimensions are given in Table 1. It may be observed that both MIL-53 and Ni/MIL-53 present a type I adsorption–desorption isotherm, characteristic to microporous materials [51]. Indeed, pore size distribution evaluated using the Horvath–Kawazoe model shows pore widths ranging between 0.4 and 2 nm in the case of both samples. As a consequence of Ni

nanoparticle deposition, the number of very small pores is reduced in the case of Ni/MIL-53, indicating either the deposition of very small Ni particles inside the pores of the MOF or the blockage of some pores due to the deposition of larger metallic particles. Specific surface area decreases from 933.2 m²/g for MIL-53 to 519.9 m²/g for Ni/MIL-53, with the corresponding decrease in specific pore volume from 0.48 cm³/g to 0.31 cm³/g, respectively, as well as of the calculated micropore volume from 0.34 cm³/g to 0.18 cm³/g.

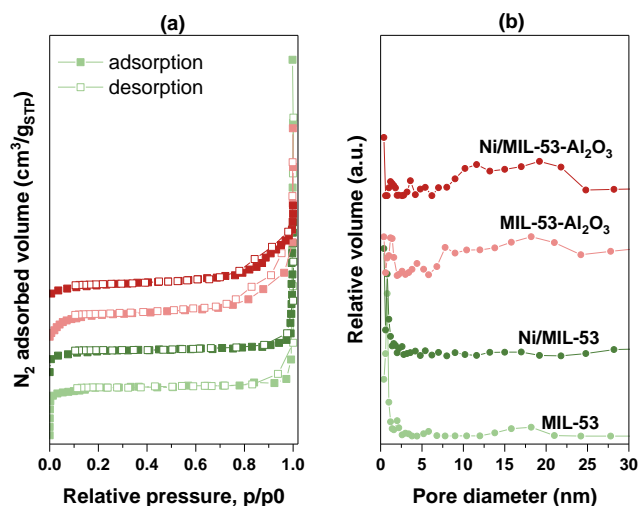


Figure 2. (a) Nitrogen adsorption–desorption isotherms and (b) pore size distribution for the MIL-53-based samples.

Table 1. Textural properties of the synthesized samples.

Sample	S _{BET} (m ² /g)	V _p (cm ³ /g)	V _μ * (cm ³ /g)	D _m (nm)
MIL-53	933.2	0.48	0.34	0.4–2
Ni(10%)/MIL-53	519.9	0.31	0.18	0.4–2
Al ₂ O ₃	110.0	0.21	-	10–25
MIL-53–Al ₂ O ₃	489.4	0.50	0.07	0.6–2.2; 3–6; 10–25
Ni(10%)/MIL-53–Al ₂ O ₃	277.9	0.42	0.03	0.6–2.8; 3–6; 12–25

* Micropore volume calculated using the t-plot method.

The adsorption–desorption isotherms of MIL-53–Al₂O₃ and Ni/MIL-53–Al₂O₃ samples combine the characteristics of both MIL-53 and Al₂O₃. Alumina, a typical mesoporous material, shows a characteristic type IV isotherm with a H2 hysteresis loop [51]. Both MIL-53–Al₂O₃-based samples exhibit the type I isotherms in the low p/p₀ region, while at higher p/p₀ values the isotherms resemble type IV more due to the characteristic hysteresis loop, proving the micro-mesoporous structure. Indeed, this combination of features originating from both MIL-53 and alumina is more evident when taking into account the pore size distribution of the MIL-53–Al₂O₃-based samples. Thus, Figure 2b shows that both MIL-53–Al₂O₃ and Ni/MIL-53–Al₂O₃ samples exhibit two types of pores: micropores ranging from 0.6 to 2.2 nm, and mesopores, some smaller in the 3–6 nm region, as well as larger ones, in the 10–25 nm domain. It should be noted, however, that Ni nanoparticle deposition on MIL-53–Al₂O₃ results in a decrease in the proportion of pores in the 0.6–2.2 region, suggesting that part of the deposited Ni fills this type of pores. Additionally, total pore volume decreases slightly upon Ni nanoparticle deposition, while calculated micropore volume is two times lower for Ni/MIL-53–Al₂O₃ as compared to MIL-53–Al₂O₃. With respect to surface area, the Ni/MIL-53–Al₂O₃ sample presents a value of 277.9 m²/g, lower than the corresponding value of 489.4 m²/g of the starting MIL-53–Al₂O₃ composite.

Morphologically, MIL-53 is composed of well-defined four-pointed star crystals (SEM image in Figure 3a), as typically reported for this MOF structure [52,53]. MIL-53 crystal growth on alumina pellets leads to the formation of MOF crystals of the same shape, which do not necessarily uniformly cover the alumina granules (Figure 3b), in contrast to the uniform coverage with MIL-101 crystals on alumina reported in our previous work in the case of the MIL-101–Al₂O₃ composite [45]. Ni deposition on the MIL-53–Al₂O₃ composite preserves the shape of the MIL-53 crystals (SEM image in Figure 3c), while TEM images presented in Figure 3d,e, with the corresponding EDS mapping, reveal a quite uniform distribution of both small (≤ 10 nm) and larger Ni particles (10–30 nm). Considering that MIL-53 does not uniformly cover the alumina pellets, Ni nanoparticles are deposited both on MIL-53 and Al₂O₃ in the case of the MIL-53–Al₂O₃ composite.

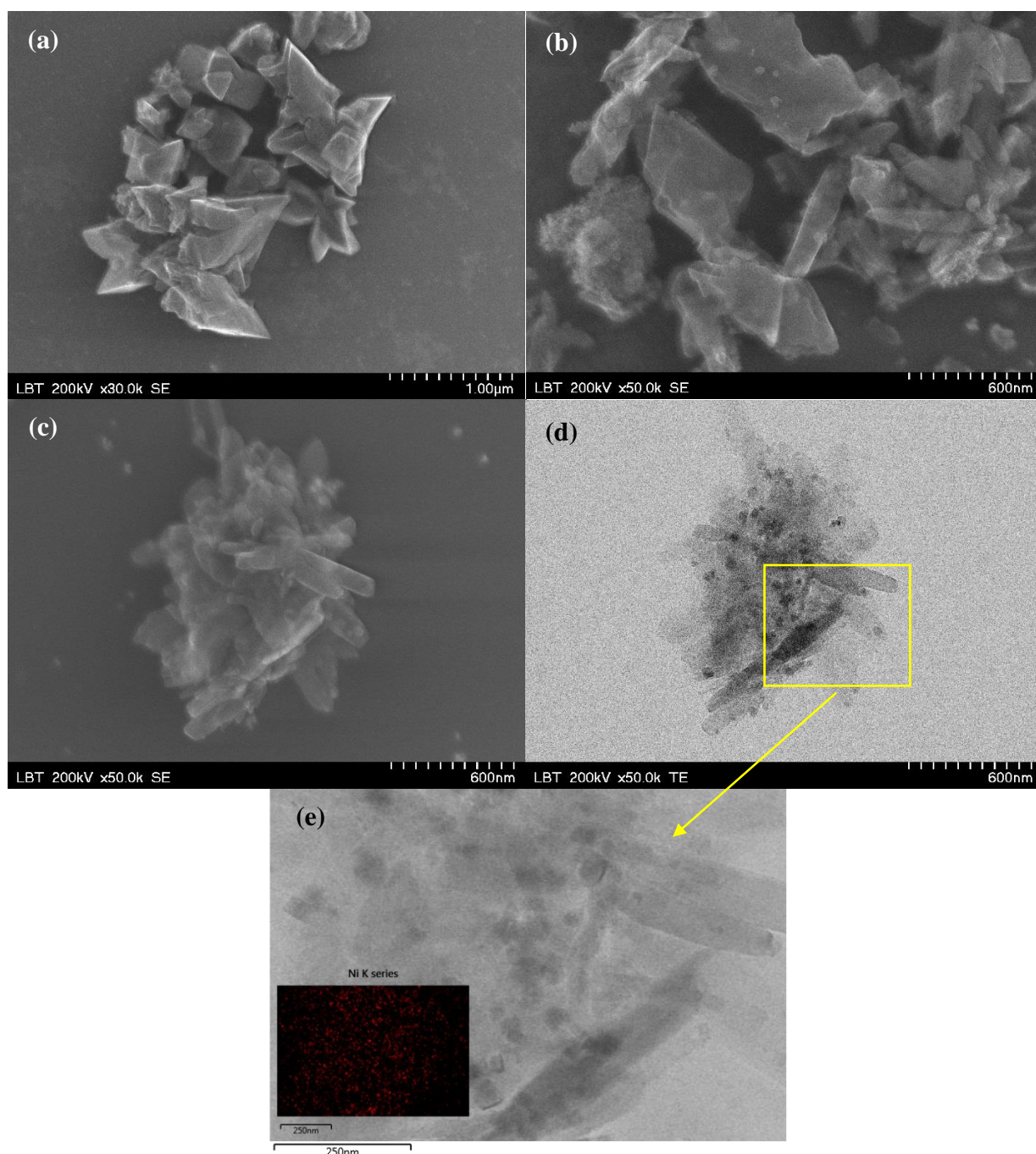


Figure 3. SEM images of (a) MIL-53, (b) MIL-53–Al₂O₃, and (c) Ni/MIL-53–Al₂O₃ and TEM images of (d), (e) Ni/MIL-53–Al₂O₃ catalyst.

Thermogravimetric analysis of MIL-53 and MIL-53–Al₂O₃ samples reveals a quite different thermal stability of the two types of materials (Figure 4). Both MIL-53 and Ni/MIL-53 samples show a first weight loss of about 5% below 120 °C due to the removal of physically adsorbed guest molecules (i.e., H₂O), and a second weight loss of 64% for MIL-53 (410 °C) and 54% for Ni/MIL-53 (390 °C) attributed to the collapse of the MOF structure due to ligand decomposition [53,54]. MIL-53–Al₂O₃ and Ni/MIL-53–Al₂O₃, on the other side, show the first weight loss of about 3% at temperatures below 120 °C, while the second weight loss occurring at temperatures above 420 °C is around 20% and 14%, respectively. The higher temperatures for the second weight loss observed from the TGA profiles indicate that both MIL-53–Al₂O₃ samples have a superior thermal stability than their MIL-53 homologues, which suggests that alumina has a stabilizing effect on MIL-53. A similar effect was evidenced in our previous work concerning MIL-101–Al₂O₃ composites [45], for which the thermal stability is, however, inferior to the one reported here for the MIL-53–Al₂O₃ samples. Moreover, TGA analysis gives important information about the temperature range, which should be considered for catalytic activity runs so that the MOF structure is not destroyed during tests. Thus, it was concluded that catalytic tests may be carried out up to 370 °C for MIL-53 samples and 420 °C for MIL-53–Al₂O₃ ones. However, in order to be able to compare the catalytic performance of the samples among each other, and also with the previously reported Ni/MIL-101–Al₂O₃ catalyst, CO₂ methanation was performed in the temperature range of 30–350 °C.

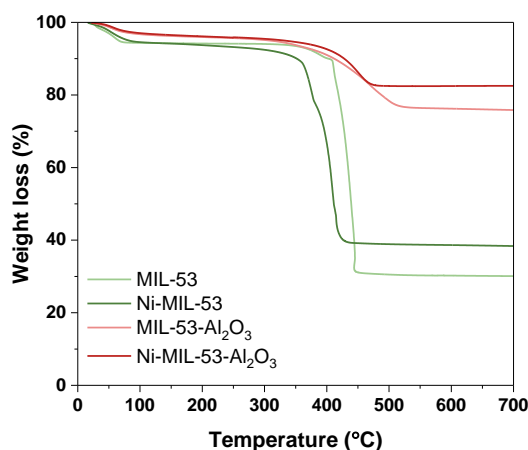


Figure 4. Thermal stability of MIL-53-based samples (TGA profiles).

2.2. Catalytic Activity Tests

2.2.1. Temperature Influence

The effect of temperature upon the catalytic performance of the studied catalysts in the CO₂ methanation process was investigated by means of temperature programmed reaction runs (TPRea), under plug flow conditions, in the temperature window of 30–350 °C. CO₂ conversion and methane selectivity profiles are comparatively presented in Figure 5 for both Ni/MIL-53 and Ni/MIL-53–Al₂O₃ catalysts, as well as the catalytic supports alone (MIL-53, MIL-53–Al₂O₃, or Al₂O₃). As expected, an increase in reaction temperature leads to an increase in CO₂ conversion in the case of Ni catalysts, while MIL-53, MIL-53–Al₂O₃, or Al₂O₃ alone show no relevant activity in the methanation of CO₂ over the entire investigated temperature domain. Ni/MIL-53 and Ni/MIL-53–Al₂O₃ samples show catalytic activity starting with temperatures as low as 250 °C. It is interesting to note that up to 300 °C, TPRea profiles show that Ni/MIL-53 is more active than Ni/MIL-53–Al₂O₃ in terms of CO₂ conversion, while at reaction temperatures above 300 °C the behavior is reversed for the two Ni catalysts (Figure 5a). Thus, at 280 °C, Ni/MIL-53 shows a CO₂ conversion value of 21.6%, while Ni/MIL-53–Al₂O₃ exhibits only 7.6%. On the other hand, at 320 °C, Ni/MIL-53–Al₂O₃ shows a CO₂ conversion of 75.6%, significantly higher than for Ni/MIL-53 at the same temperature, that is 51.9%. Both MIL-53-based catalysts show

maximum CO₂ conversion values at 350 °C: 75.5% for Ni/MIL-53 and 88.8% for Ni/MIL-53–Al₂O₃. In terms of temperature for half CO₂ conversion ($T_{50\%}$), there are no significant differences between the two Ni catalysts, since $T_{50\%} = 312$ °C for Ni/MIL-53–Al₂O₃ and $T_{50\%} = 320$ °C for Ni/MIL-53.

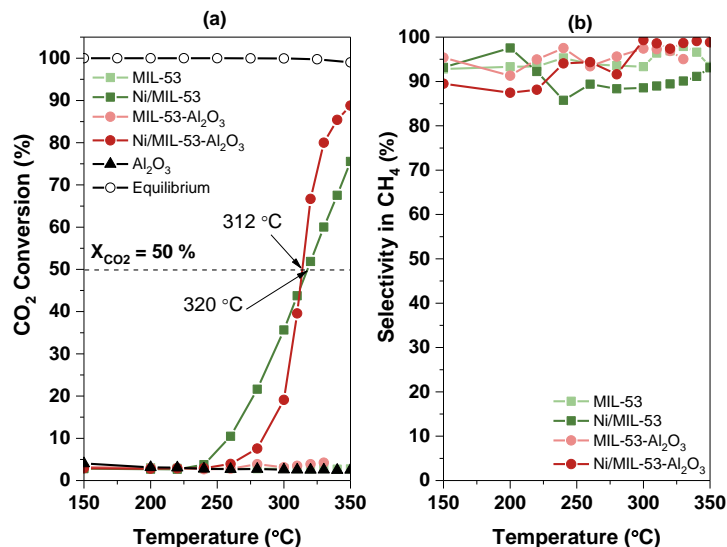


Figure 5. Temperature influence on the catalytic performance of the MIL-53-based samples in the methanation of CO₂: (a) CO₂ conversion and (b) methane selectivity (CO₂:H₂ = 1:5.2; [CO₂] = 6.6%, $p = 1$ atm, 2 °C/min, 4650 h^{−1}).

Selectivity to methane is above 85% in the case of both catalysts over the entire temperature range; however, Ni/MIL-53–Al₂O₃ shows slightly superior selectivity values of 94–99%, as compared to 86–93% for Ni/MIL-53, at reaction temperatures above 250 °C (Figure 5b).

Methane turnover frequency (TOF) values, defined as moles of formed methane/moles of Ni/time, were calculated under differential reaction conditions, that is, conversion of CO₂ below 25%. It should be noted here that each Ni particle was considered accessible by the species of interest, since the metal surface area is difficult to determine for metal/MOF catalysts. This is due to the fact during H₂ chemisorption analysis, as usually employed for metal surface area determination, one cannot accurately discriminate between the amount of hydrogen adsorbed on the active metal sites and the amount of hydrogen adsorbed in the MOF scaffold (one of the first explored applications for MOFs was actually the adsorption and storage of H₂). This means that methane turnover frequencies presented here are actually underestimated. Even so, the obtained values still highlight the catalytic potential of MIL-53-based catalysts. Thus, at 220 °C, Ni/MIL-53 shows a TOF value of $1.22 \times 10^{-4} \text{ s}^{-1}$, while Ni/MIL-53–Al₂O₃ presents a value only slightly superior, $1.27 \times 10^{-4} \text{ s}^{-1}$. However, at 280 °C, Ni/MIL-53 reveals a TOF value almost three times larger than that corresponding to Ni/MIL-53–Al₂O₃ ($8.44 \times 10^{-4} \text{ s}^{-1}$ compared to $3.07 \times 10^{-4} \text{ s}^{-1}$). These TOF values are similar or larger than TOF values determined at the same temperature (280 °C) for the very few MOF-based Ni catalysts reported in the literature to have been investigated for the CO₂ methanation process: $0.9 \times 10^{-4} \text{ s}^{-1}$ [22] or $2.21 \times 10^{-4} \text{ s}^{-1}$ [28] for Ni(10%)/MIL-101(DS), or $8.05 \times 10^{-4} \text{ s}^{-1}$ for the Ni/MIL-101–Al₂O₃ catalyst [45]. MIL-53 catalysts presented in this work reveal a different behavior as compared to their MIL-101 homologues reported previously [45], for which the Ni/MIL-101–Al₂O₃ catalyst revealed net superior catalytic performance parameters (CO₂ conversion, $T_{50\%}$, or TOF) compared to Ni/MIL-101 over the entire investigated temperature range. This peculiar behavior of Ni/MIL-53–Al₂O₃ compared to Ni/MIL-53 is most probably due to the less pronounced synergistic effect occurring between MIL-53 and alumina as a consequence of irregular MOF growth on the alumina pellets. Compared to the case of the MIL-101–Al₂O₃ composite, a lower affinity of

MIL-53 to the alumina was observed, which leads to a less intimate interaction between alumina and MIL-53.

2.2.2. Stability Tests

Ni/MIL-53 and Ni/MIL-53-Al₂O₃ were subjected to stability tests in the methanation of CO₂ at 280 °C, with all other reaction conditions identical to those employed in the TPRea runs. In the case of Ni/MIL-53, approximately 20 min time on stream (TOS) is needed to attain steady-state CO₂ conversion and CH₄ selectivity values, while for Ni/MIL-53-Al₂O₃ stability is attained only after approximately 90 min TOS (Figure 6). Interestingly, both Ni catalysts present superior catalytic activity values than those determined from TPRea runs at the same temperature, with peculiar differences among them, however. In the case of Ni/MIL-53, stability values are only slightly larger than those evaluated from TPRea tests: CO₂ conversion around 23% compared to 21.6%. Ni/MIL-53-Al₂O₃, on the other hand, shows almost seven times larger stable CO₂ conversion values, around 52–53%, as compared to 7.6% obtained at 280 °C during TPRea runs. Moreover, CH₄ selectivity values stabilize around 94% for Ni/MIL-53 and 97% for Ni/MIL-53-Al₂O₃, with both values higher than the corresponding ones determined during TPRea tests. One possible explanation for this different behavior between TPRea and stability tests is the fact that a 2 °C/min temperature rate, although low, does not allow stabilization at each temperature value, and therefore, catalytic activity parameters evaluated from TPRea runs are transient ones. However, this fact is not sufficient to explain the low differences observed in the case of Ni/MIL-53, and the significantly larger ones in the case of Ni/MIL-53-Al₂O₃. Another possible explanation would be the effect of the presence of larger Ni particles on the MIL-53-Al₂O₃ composite, besides the very small ones, considering that CO₂ methanation is favored neither by very small metal particles nor by very large ones [1].

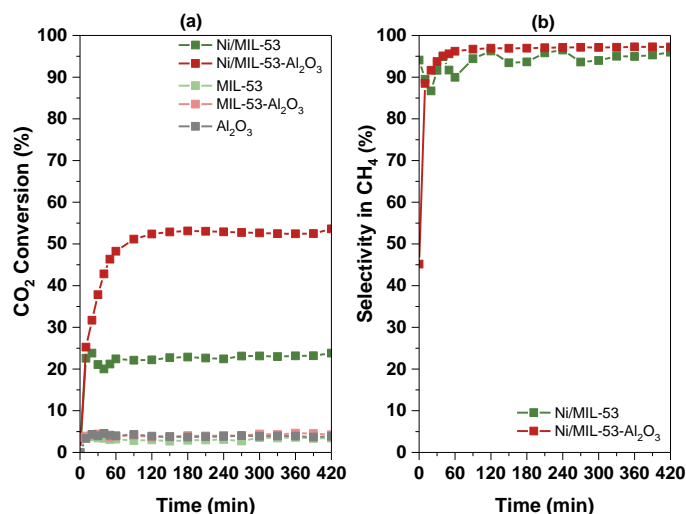


Figure 6. Stability of Ni/MIL-53 and Ni/MIL-53-Al₂O₃ catalysts in the methanation of CO₂ at 280 °C: (a) conversion of CO₂ and (b) CH₄ selectivity (CO₂:H₂ = 1:5.2; [CO₂] = 6.6%, *p* = 1 atm, 4650 h⁻¹).

Characterization by powder X-ray diffraction of used catalysts during stability tests performed at 280 °C reveals their good stability under prolonged exposure to the reaction medium. Thus, XRD patterns illustrated in Figure 7 show that the structure and crystallinity of MIL-53 deposited on the alumina pellets are very well preserved, either in the used MIL-53-Al₂O₃ composite alone or the corresponding Ni catalyst. This feature, together with the good thermal stability of the MIL-53-based catalysts, makes Ni/MIL-53 and Ni/MIL-53-Al₂O₃ promising candidates for the CO₂ methanation process.

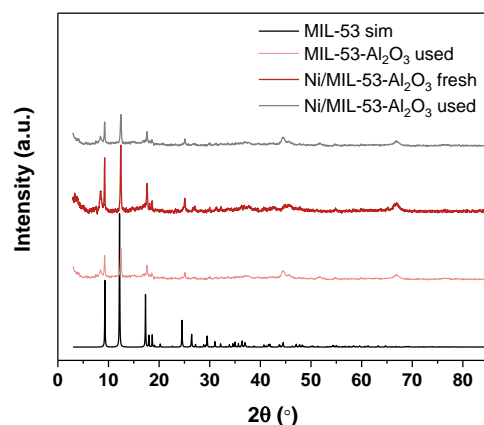


Figure 7. Comparative XRD patterns for the fresh and used Ni/MIL-53–Al₂O₃ samples.

Corroborating the results obtained during catalytic activity investigations (TPRea and stability tests), it might be concluded that Ni/MIL-53–Al₂O₃ shows better catalytic performance than Ni/MIL-53 in the methanation of CO₂. Comparison with their previously reported MIL-101 homologues [45], tested under the same reaction conditions (low GHSV of 4650 h^{−1} and excess of H₂), leads us to the conclusion that catalytic activity in the investigated reaction increases in the series: Ni/MIL-53 < Ni/MIL-101 < Ni/MIL-53–Al₂O₃ < Ni/MIL-101–Al₂O₃. Although not superior to Ni/MIL-101–Al₂O₃ in terms of catalytic activity, the performance of Ni/MIL-53–Al₂O₃ in CO₂ methanation proves once more the real potential of using MOFs for catalytic applications by their immobilization on cheap and mechanically more stable supports such as alumina.

3. Materials and Methods

3.1. Chemicals and Gases

All chemicals and gases were purchased from commercial suppliers and used as such. Benzene-1,4-dicarboxylic acid (BDC), N,N-dimethylformamide (DMF), and nickel nitrate hexahydrate (Ni(NO₃)₂·6H₂O) were purchased from Merck (Darmstadt, Germany), chromium chloride hexahydrate (CrCl₃·6H₂O) from Sigma Aldrich (Steinheim, Germany), alumina (Al₂O₃) from Alfa Aesar (Karlsruhe, Germany), and gases (Ar, and gas mixtures: CO₂ in Ar, H₂ and Ar) from Linde Gaz Romania (Cluj Napoca, Romania).

3.2. MIL-53 and MIL-53–Al₂O₃ Synthesis

Synthesis of MIL-53 was achieved by means of an adapted synthesis method, using only water as solvent, with no added HF as used in the classical procedure [47], while the reaction time is reduced from 72 h to 12 h. Thus, an equimolar mixture of reactants (4.35 mmol BDC and 4.35 mmol CrCl₃·6H₂O), mixed with 5 mL distilled water, was heated at 190 °C for 12 h in an electric oven, using a Teflon-lined stainless-steel autoclave. After cooling to room temperature, the product was filtered using a fritted funnel and washed with distilled water several times. The obtained solid was dried at 100 °C for 12 h, activated under reflux of dimethylformamide (DMF) for 24 h in order to remove the unreacted BDC trapped in the pores of the MOF, filtered again, and dried at 150 °C for 12 h. In order to obtain the low-temperature form of MIL-53, the dried sample was heat-treated by 1 °C/min up to 300 °C, under air, for 24 h, and then cooled naturally to room temperature.

MIL-53–Al₂O₃ was obtained by crystallization of MIL-53 on alumina particles (commercial alumina, 110 m²/g, 0.21 cm³/g, d_p > 0.125 mm), using the same mixture of reactants as in the case of MIL-53 alone. Thus, 0.3 g alumina, the equimolar mixture of BDC and CrCl₃·6H₂O (4.35 mmol each), and water (5 mL) were heated at 150 °C for 12 h in a Teflon-lined stainless-steel autoclave. After cooling, the solid was separated from the liquid phase by decantation, and washed with water several times. The separated solid was further dried in an electric oven at 150 °C for 12 h. The dried granules of MIL-53-coated

alumina were activated in dimethylformamide (DMF) under reflux for 24 h, filtered, and then dried for 12 h at 150 °C. As in the case of MIL-53 alone, the obtained composite MIL-53–Al₂O₃ was heat-treated in air for 24 h at 300 °C (1 °C/min), and then cooled down to room temperature.

3.3. Preparation of Ni/MIL-53 and Ni/MIL-53–Al₂O₃ Catalysts

Before deposition of Ni nanoparticles, the pores of both MIL-53 and MIL-53–Al₂O₃ were cleared by drying at 300 °C (2 h). In order to deposit the Ni nanoparticles of interest in the pores of MIL-53, instead of on its outer surface, an adapted “double solvent method” (DS) was used [28,55] for both MIL-53 and MIL-53–Al₂O₃. In principle, two solvents are used to achieve this goal: a nonpolar solvent (i.e., n-hexane) is used to make the outer surface of the catalytic support hydrophobic, while a polar solvent (i.e., water) is used to dissolve the metallic precursor and to orient it to the hydrophilic pores of the support.

In order to prepare Ni/MIL-53 catalyst, 0.3 g of dried MIL-53 was dispersed in hexane (60 mL) in a round bottom flask, after cleaning the flask with Ar in order to remove the air. Homogeneous dispersion of MIL-53 in hexane was achieved by sonication for 30 min, and then magnetic stirring (500 rpm, 30 min). In order to obtain the targeted 10 wt.% Ni loading, a volume of Ni(NO₃)₂ aqueous solution equal to the pore volume of the support was prepared and added dropwise over the dispersed MOF, and then stirred for 30 min. The remaining clear hexane over the impregnated MIL-53 was removed by decantation. Reduction to metallic Ni was performed by NaBH₄ aqueous solution (3M): a solution volume equal to 5 times the pore volume of the initial amount of MIL-53 was added in fine drops over the impregnated MIL-53 dispersed in water (60 mL). The mixture was stirred for 15 min, then filtered, and thoroughly washed with distilled water. The Ni/MIL-53 sample thus obtained was further dried overnight at room temperature, and then dried for 3 h in an electric oven at 150 °C.

Synthesis of Ni/MIL-53–Al₂O₃ catalyst was performed following the same procedure as for Ni/MIL-53, apart from the sonication step of the support in hexane, which was avoided in order to ensure that the deposited MOF on alumina is not removed during this step.

3.4. Characterization Techniques

X-ray powder diffraction (XRD) analyses were carried out using a Bruker D8 Advance Diffractometer (Billerica, MA, USA), with the X-ray tube operating at 40 kV and 40 mA and equipped with a germanium monochromator to obtain CuK α ₁ radiation. The diffractograms were recorded in the 385° 2 θ range, with a scan rate of 0.01°/s. Nitrogen physisorption isotherms at –196 °C (Sorptomatic 1990, Thermo Electron, Milan, Italy) were used to estimate the specific surface area (BET method, p/p₀ = 0.01–0.25), pore volume (p/p₀ = 0.95), and pore size distribution of the prepared samples. The t-plot method was used to estimate the micropore volume of samples (de Boer statistical thickness of 3.0–6.5 Å). Pretreatment of samples before N₂ adsorption consisted of degassing at 200 °C, under vacuum, for 4 h. Thermogravimetric analysis (TGA) was carried out in air (100 mL/min), in the temperature range of 25–700 °C, with a 10 °C/min temperature rate (SDT Q600, TA Instruments, New Castle, DE, USA). A HITACHI HD-2700 STEM microscope (Hitachi, Tokyo, Japan) operating at 200 kV was used for scanning electron microscopy (SEM), transmission electron microscopy (TEM), and energy dispersive X-ray (EDX) analyses. Each catalyst sample was dispersed in ethanol by sonication (3 min) before SEM/TEM analyses.

3.5. Catalytic Measurements

The performance of the MIL-53 catalysts in the methanation process was evaluated using an experimental set-up comprised of the TPDR0 1100 Series instrument (Thermo Scientific, Milan, Italy) coupled to the PrismaPlus quadrupole mass spectrometer (Pfeiffer Vacuum, Asslar, Germany). Temperature influence on the catalytic activity was investigated

in the 30–350 °C range by temperature programmed reactions (TPRea, 2 °C/min), while stability tests were performed at 280 °C. Catalyst samples of 0.1 g were placed in a fixed-bed quartz reactor (i.d. 10 mm) between two alumina wool pads. In order to ensure the same flow conditions for each catalytic run, that is the same height of the catalytic bed, catalyst samples based on MIL-53–Al₂O₃ composite were diluted with alumina as necessary. The total flow of the inlet gases was set to 31 mL/min (GHSV = 4650 h⁻¹), with a composition of 6.6% CO₂, 34.5% H₂, and Ar as balance gas (CO₂:H₂ = 1:5.2). For comparative reasons, these reaction conditions are identical to the ones used for the previously reported Ni/MIL-101–Al₂O₃ and Ni/MIL-101 catalysts [45]. The dry effluent gases (reactants and products) were analyzed by the coupled MS by monitoring the following components: H₂ (*m/z* = 2), CH₄ (*m/z* = 15), H₂O (*m/z* = 18), CO (*m/z* = 28), and CO₂ (*m/z* = 44). Interference with other species was avoided in case of methane by selecting mass number 15 instead of 16 [56]. Catalytic activity parameters such as CO₂ conversion and CH₄ selectivity were calculated using the output MS signals for the species of interest, considering that the intensity of the signals is proportional to the concentration of each species in the analyzed mixture. Thus, the following relationships were used (with the signal for mass number 28 corrected in order to eliminate the contribution of CO₂, and of the residual air, and therefore to account only for CO):

$$X_{\text{CO}_2} = \left(1 - \frac{I_{\text{CO}_2}^{\text{out}}}{I_{\text{CO}_2}^{\text{out}} + I_{\text{CH}_4}^{\text{out}} + I_{\text{CO}}^{\text{out}}} \right) \times 100, (\%) \quad (1)$$

$$Y_{\text{CH}_4} = \frac{I_{\text{CH}_4}^{\text{out}}}{I_{\text{CO}_2}^{\text{out}} + I_{\text{CH}_4}^{\text{out}} + I_{\text{CO}}^{\text{out}}} \times 100, (\%) \quad (2)$$

$$S_{\text{CH}_4} = \frac{Y_{\text{CH}_4}}{X_{\text{CO}_2}} \times 100, (\%) \quad (3)$$

4. Conclusions

MIL-53(Cr), a MOF structure from the benzenedicarboxylates family with better thermal and chemical stability than MIL-101 in the same family, was immobilized on commercial alumina pellets using a solvothermal method involving only water as the solvent, besides CrCl₃ and benzene-1,4-dicarboxylic acid as reagents. The obtained MIL-53–Al₂O₃ composite, which combines the porosity characteristics of both MIL-53 and alumina, was used as a catalytic support for the deposition of Ni nanoparticles using an impregnation method with two solvents. The Ni/MIL-53–Al₂O₃ catalyst was compared to its homologue Ni/MIL-53 in terms of structural and morphological properties, as well as the catalytic activity in the methanation of CO₂.

Ni nanoparticle deposition on both MIL-53 and MIL-53–Al₂O₃ leads to a relatively uniform dispersion of metallic particles, both larger (10–30 nm) and smaller (≤10 nm) ones. The structure of MIL-53 or the MIL-53–Al₂O₃ composite is retained after the deposition of Ni nanoparticles, while the thermal stability of both the MIL-53–Al₂O₃ composite and Ni/MIL-53–Al₂O₃ catalyst outperforms that of the MIL-53 counterparts.

Catalytic activity tests performed under plug flow conditions in TPRea experiments in the 30–350 °C temperature range showed that Ni/MIL-53 presents better performances in terms of CO₂ conversion, CH₄ selectivity, or TOF value at reaction temperatures below 300 °C, while above this temperature Ni/MIL-53–Al₂O₃ is superior. However, under steady-state conditions during stability tests at 280 °C, Ni/MIL-53–Al₂O₃ shows a CO₂ conversion of 52% (2.5 times higher than in the case of Ni/MIL-53), with a corresponding CH₄ selectivity of 97%. Moreover, the structure and crystallinity of MIL-53 are preserved in all samples after stability tests. It may be concluded that Ni/MIL-53–Al₂O₃ is more active in the methanation of CO₂ than its counterpart Ni/MIL-53. Thus, Ni/MIL-53–Al₂O₃ proves once more the potential of using MOFs for catalytic applications by immobilization on cheap and more mechanically stable supports such as alumina.

Author Contributions: Conceptualization, O.G., G.B. and M.M.; methodology, O.G., M.D.L. and M.M.; validation, G.B. and M.M.; formal analysis, M.M.; investigation, O.G. and M.M.; resources, M.M.; data curation, M.D.L. and M.M.; writing—original draft preparation, M.M.; writing—review and editing, M.M.; visualization, O.G., M.D.L. and M.M.; supervision, M.M.; project administration, M.M.; funding acquisition, M.M. All authors have read and agreed to the published version of the manuscript.

Funding: This work was supported by grants of the Romanian Ministry of Education and Research, CNCS-UEFISCDI, project number PN-III-P1-1.1-PD-2016-1228 and PN-III-P1-1.1-TE-2019-1447, within PNCDI III. TEM/SEM/EDX measurements were partially supported through the infrastructure obtained in the Project: Research Center and Advanced Technologies for Alternative Energies – CETATEA – 623/11.03.2014.

Data Availability Statement: The raw/processed data required to reproduce these findings cannot be shared at this time as the data also form part of an ongoing study.

Acknowledgments: The contributions of Lucian Barbu-Tudoran for the TEM/SEM/EDX analyses and of Monica Dan for the TGA measurements are gratefully acknowledged.

Conflicts of Interest: The authors declare no conflict of interest. The funders had no role in the design of the study; in the collection, analyses, or interpretation of data; in the writing of the manuscript, or in the decision to publish the results.

References

1. Vogt, C.; Groeneveld, E.; Kamsma, G.; Nachtegaal, M.; Lu, L.; Kiely, C.; Berben, P.H.; Meirer, F.; Weckhuysen, B.M. Unravelling structure sensitivity in CO₂ hydrogenation over nickel. *Nat. Catal.* **2018**, *1*, 127–134. [[CrossRef](#)]
2. Aresta, M.; Dibenedetto, A.; Angelini, A. Catalysis for the Valorization of Exhaust Carbon: From CO₂ to Chemicals, Materials, and Fuels. Technological Use of CO₂. *Chem. Rev.* **2013**, *114*, 1709–1742. [[CrossRef](#)] [[PubMed](#)]
3. Ghaib, K.; Ben-Fares, F.-Z. Power-to-Methane: A state-of-the-art review. *Renew. Sustain. Energy Rev.* **2018**, *81*, 433–446. [[CrossRef](#)]
4. Meylan, F.D.; Moreau, V.; Erkman, S. CO₂ utilization in the perspective of industrial ecology, an overview. *J. CO₂ Util.* **2015**, *12*, 101–108. [[CrossRef](#)]
5. Najafabadi, A.T. CO₂ chemical conversion to useful products: An engineering insight to the latest advances toward sustainability. *Int. J. Energy Res.* **2013**, *37*, 485–499. [[CrossRef](#)]
6. Bahari, N.A.; Isahak, W.N.R.W.; Masdar, M.S.; Yaakob, Z. Clean hydrogen generation and storage strategies via CO₂ utilization into chemicals and fuels: A review. *Int. J. Energy Res.* **2019**, *43*, 5128–5150. [[CrossRef](#)]
7. Murena, F.; Esposito, S.; Deorsola, F.; Galletti, C.; Prati, M. CO₂ abatement and CH₄ recovery at vehicle exhausts: Comparison and characterization of Ru powder and pellet catalysts. *Int. J. Hydrogen Energy* **2020**, *45*, 8640–8648. [[CrossRef](#)]
8. Fechete, I.; Vedrine, J.C. Nanoporous Materials as New Engineered Catalysts for the Synthesis of Green Fuels. *Molecules* **2015**, *20*, 5638–5666. [[CrossRef](#)]
9. Lee, W.J.; Li, C.; Prajitno, H.; Yoo, J.; Patel, J.; Yang, Y.; Lim, S. Recent trend in thermal catalytic low temperature CO₂ methanation: A critical review. *Catal. Today* **2020**, *368*, 2–19. [[CrossRef](#)]
10. Frontera, P.; Macario, A.; Ferraro, M.; Antonucci, P. Supported Catalysts for CO₂ Methanation: A Review. *Catalysts* **2017**, *7*, 59. [[CrossRef](#)]
11. Kim, A.; Sanchez, C.; Haye, B.; Boissière, C.; Sassoye, C.; Debecker, D.P. Mesoporous TiO₂ Support Materials for Ru-Based CO₂ Methanation Catalysts. *ACS Appl. Nano Mater.* **2019**, *2*, 3220–3230. [[CrossRef](#)]
12. Karam, L.; Bacariza, M.C.; Lopes, J.M.; Henriques, C.; Reboul, J.; El Hassan, N.; Massiani, P. Mesoporous nickel-alumina catalysts derived from MIL-53(Al) metal-organic framework: A new promising path for synthesizing CO₂ methanation catalysts. *J. CO₂ Util.* **2021**, *51*, 101651. [[CrossRef](#)]
13. Liang, C.; Hu, X.; Wei, T.; Jia, P.; Zhang, Z.; Dong, D.; Zhang, S.; Liu, Q.; Hu, G. Methanation of CO₂ over Ni/Al₂O₃ modified with alkaline earth metals: Impacts of oxygen vacancies on catalytic activity. *Int. J. Hydrogen Energy* **2019**, *44*, 8197–8213. [[CrossRef](#)]
14. Renda, S.; Ricca, A.; Palma, V. Study of the effect of noble metal promotion in Ni-based catalyst for the Sabatier reaction. *Int. J. Hydrogen Energy* **2020**, *46*, 12117–12127. [[CrossRef](#)]
15. Mihet, M.; Lazar, M.D. Methanation of CO₂ on Ni/ γ -Al₂O₃: Influence of Pt, Pd or Rh promotion. *Catal. Today* **2018**, *306*, 294–299. [[CrossRef](#)]
16. Mutz, B.; Carvalho, H.W.; Mangold, S.; Kleist, W.; Grunwaldt, J.-D. Methanation of CO₂: Structural response of a Ni-based catalyst under fluctuating reaction conditions unraveled by operando spectroscopy. *J. Catal.* **2015**, *327*, 48–53. [[CrossRef](#)]
17. Kim, H.Y.; Lee, H.M.; Park, J.-N. Bifunctional Mechanism of CO₂ Methanation on Pd-MgO/SiO₂ Catalyst: Independent Roles of MgO and Pd on CO₂ Methanation. *J. Phys. Chem. C* **2010**, *114*, 7128–7131. [[CrossRef](#)]
18. Duyar, M.; Treviño, M.A.; Farrauto, R.J. Dual function materials for CO₂ capture and conversion using renewable H₂. *Appl. Catal. B Environ.* **2015**, *168–169*, 370–376. [[CrossRef](#)]

19. Mihet, M.; Dan, M.; Barbu-Tudoran, L.; Lazar, M.D. CO₂ Methanation Using Multimodal Ni/SiO₂ Catalysts: Effect of Support Modification by MgO, CeO₂, and La₂O₃. *Catalysts* **2021**, *11*, 443. [[CrossRef](#)]
20. Moon, H.R.; Lim, D.-W.; Suh, M.P. Fabrication of metal nanoparticles in metal–organic frameworks. *Chem. Soc. Rev.* **2012**, *42*, 1807–1824. [[CrossRef](#)]
21. Cui, W.-G.; Zhang, G.-Y.; Hu, T.-L.; Bu, X.-H. Metal-organic framework-based heterogeneous catalysts for the conversion of C1 chemistry: CO, CO₂ and CH₄. *Coord. Chem. Rev.* **2019**, *387*, 79–120. [[CrossRef](#)]
22. Zhen, W.; Gao, F.; Tian, B.; Ding, P.; Deng, Y.; Li, Z.; Gao, H.; Lu, G. Enhancing activity for carbon dioxide methanation by encapsulating (1 1 1) facet Ni particle in metal–organic frameworks at low temperature. *J. Catal.* **2017**, *348*, 200–211. [[CrossRef](#)]
23. Wang, H.; Zhu, Q.-L.; Zou, R.; Xu, Q. Metal-Organic Frameworks for Energy Applications. *Chem* **2017**, *2*, 52–80. [[CrossRef](#)]
24. Chen, Y.-Z.; Zhang, R.; Jiao, L.; Jiang, H.-L. Metal–organic framework-derived porous materials for catalysis. *Coord. Chem. Rev.* **2018**, *362*, 1–23. [[CrossRef](#)]
25. Gascon, J.; Corma, A.; Kapteijn, F.; Llabres i Xamena, F.X. Metal Organic Framework Catalysis: Quo vadis? *ACS Catal.* **2014**, *4*, 361–378. [[CrossRef](#)]
26. Falcaro, P.; Ricco, R.; Yazdi, A.; Imaz, I.; Furukawa, S.; Maspoch, D.; Ameloot, R.; Evans, J.D.; Doonan, C.J. Application of metal and metal oxide nanoparticles@MOFs. *Coord. Chem. Rev.* **2016**, *307*, 237–254. [[CrossRef](#)]
27. Zhen, W.; Li, B.; Lu, G.; Ma, J. Enhancing catalytic activity and stability for CO₂ methanation on Ni@MOF-5 via control of active species dispersion. *Chem. Commun.* **2014**, *51*, 1728–1731. [[CrossRef](#)]
28. Mihet, M.; Grad, O.; Blanita, G.; Radu, T.; Lazar, M.D. Effective encapsulation of Ni nanoparticles in metal-organic frameworks and their application for CO₂ methanation. *Int. J. Hydrogen Energy* **2019**, *44*, 13383–13396. [[CrossRef](#)]
29. Zhao, Z.-W.; Zhou, X.; Liu, Y.-N.; Shen, C.-C.; Yuan, C.-Z.; Jiang, Y.-F.; Zhao, S.-J.; Ma, L.-B.; Cheang, T.-Y.; Xu, A.-W. Ultrasmall Ni nanoparticles embedded in Zr-based MOFs provide high selectivity for CO₂ hydrogenation to methane at low temperatures. *Catal. Sci. Technol.* **2018**, *8*, 3160–3165. [[CrossRef](#)]
30. Mihet, M.; Blanita, G.; Dan, M.; Barbu-Tudoran, L.; Lazar, M.D. Pt/UIO-66 Nanocomposites as Catalysts for CO₂ Methanation Process. *J. Nanosci. Nanotechnol.* **2019**, *19*, 3187–3196. [[CrossRef](#)]
31. Xie, Z.; Xu, W.; Cui, X.; Wang, Y. Recent Progress in Metal-Organic Frameworks and Their Derived Nanostructures for Energy and Environmental Applications. *ChemSusChem* **2017**, *10*, 1645–1663. [[CrossRef](#)]
32. Bazer-Bachi, D.; Assié, L.; Lecocq, V.; Harbuzaru, B.; Falk, V. Towards industrial use of metal-organic framework: Impact of shaping on the MOF properties. *Powder Technol.* **2014**, *255*, 52–59. [[CrossRef](#)]
33. Li, Z.; Zeng, H.C. Armored MOFs: Enforcing Soft Microporous MOF Nanocrystals with Hard Mesoporous Silica. *J. Am. Chem. Soc.* **2014**, *136*, 5631–5639. [[CrossRef](#)] [[PubMed](#)]
34. Blanita, G.; Mihet, M.; Borodi, G.; Misan, I.; Coldea, I.; Lupu, D. Ball milling and compression effects on hydrogen adsorption by MOF:Pt/carbon mixtures. *Microporous Mesoporous Mater.* **2015**, *203*, 195–201. [[CrossRef](#)]
35. Ramos-Fernandez, E.V.; Garcia-Domingos, M.; Juan-Alcañiz, J.; Gascon, J.; Kapteijn, F. MOFs meet monoliths: Hierarchical structuring metal organic framework catalysts. *Appl. Catal. A Gen.* **2011**, *391*, 261–267. [[CrossRef](#)]
36. Furukawa, S.; Reboul, J.; Diring, S.; Sumida, K.; Kitagawa, S. Structuring of metal–organic frameworks at the mesoscopic/macroscopic scale. *Chem. Soc. Rev.* **2014**, *43*, 5700–5734. [[CrossRef](#)] [[PubMed](#)]
37. Song, X.; Guan, Q.; Cheng, Z.; Li, W. Eco-friendly controllable synthesis of highly dispersed ZIF-8 embedded in porous Al₂O₃ and its hydrogenation properties after encapsulating Pt nanoparticles. *Appl. Catal. B Environ.* **2018**, *227*, 13–23. [[CrossRef](#)]
38. Górka, J.; Fulvio, P.F.; Pikus, S.; Jaroniec, M. Mesoporous metal organic framework–boehmite and silica composites. *Chem. Commun.* **2010**, *46*, 6798–6800. [[CrossRef](#)]
39. Hermes, S.; Zacher, D.; Baunemann, A.; Wöll, C.; Fischer, R.A. Selective Growth and MOCVD Loading of Small Single Crystals of MOF-5 at Alumina and Silica Surfaces Modified with Organic Self-Assembled Monolayers†. *Chem. Mater.* **2007**, *19*, 2168–2173. [[CrossRef](#)]
40. Buso, D.; Nairn, K.M.; Gimona, M.; Hill, A.J.; Falcaro, P. Fast Synthesis of MOF-5 Microcrystals Using Sol–Gel SiO₂ Nanoparticles. *Chem. Mater.* **2011**, *23*, 929–934. [[CrossRef](#)]
41. Karimi, Z.; Morsali, A. Modulated formation of metal-organic frameworks by oriented growth over mesoporous silica. *J. Mater. Chem. A* **2013**, *1*, 3047–3054. [[CrossRef](#)]
42. Furtado, A.M.B.; Liu, J.; Wang, Y.; LeVan, M.D. Mesoporous silica–metal organic composite: Synthesis, characterization, and ammonia adsorption. *J. Mater. Chem.* **2011**, *21*, 6698–6706. [[CrossRef](#)]
43. Ameloot, R.; Liekens, A.; Alaerts, L.; Maes, M.; Galarneau, A.; Coq, B.; Desmet, G.; Sels, B.F.; Denayer, J.; De Vos, D.E. Silica-MOF Composites as a Stationary Phase in Liquid Chromatography. *Eur. J. Inorg. Chem.* **2010**, *2010*, 3735–3738. [[CrossRef](#)]
44. Liu, Y.; Ng, Z.; Khan, E.A.; Jeong, H.-K.; Ching, C.-B.; Lai, Z. Synthesis of continuous MOF-5 membranes on porous α -alumina substrates. *Microporous Mesoporous Mater.* **2009**, *118*, 296–301. [[CrossRef](#)]
45. Grad, O.; Mihet, M.; Blanita, G.; Dan, M.; Barbu-Tudoran, L.; Lazar, M.D. MIL-101-Al₂O₃ as catalytic support in the methanation of CO₂—Comparative study between Ni/MIL-101 and Ni/MIL-101-Al₂O₃ catalysts. *Catal. Today* **2020**, *366*, 114–122. [[CrossRef](#)]
46. Cao, N.; Su, J.; Luo, W.; Cheng, G. Ni–Pt nanoparticles supported on MIL-101 as highly efficient catalysts for hydrogen generation from aqueous alkaline solution of hydrazine for chemical hydrogen storage. *Int. J. Hydrogen Energy* **2014**, *39*, 9726–9734. [[CrossRef](#)]

47. Serre, C.; Millange, F.; Thouvenot, C.; Nogues, M.; Louer, D.; Férey, G. Very Large Breathing Effect in the First Nanoporous Chromium (III)-Based Solids: MIL-53 or $\text{CrIII}(\text{OH})_2(\text{O}_2\text{C}-\text{C}_6\text{H}_4-\text{CO}_2)_x(\text{HO}_2\text{C}-\text{C}_6\text{H}_4-\text{CO}_2\text{H})_y \cdot x\text{H}_2\text{O}$. *J. Am. Chem. Soc.* **2002**, *124*, 13519–13526. [[CrossRef](#)]
48. Bourrelly, S.; Llewellyn, P.L.; Serre, C.; Millange, F.; Loiseau, T.; Férey, G. Different adsorption behaviors of methane and carbon dioxide in the isotopic nanoporous metal terephthalates MIL-53 and MIL-47. *J. Am. Chem. Soc.* **2005**, *127*, 13519–13521. [[CrossRef](#)]
49. Llewellyn, P.L.; Bourrelly, S.; Serre, C.; Filinchuk, Y.; Férey, G. How Hydration Drastically Improves Adsorption Selectivity for CO_2 over CH_4 in the Flexible Chromium Terephthalate MIL-53. *Angew. Chem.* **2006**, *118*, 7915–7918. [[CrossRef](#)]
50. Zhao, X.; Jin, Y.; Zhang, F.; Zhong, Y.; Zhu, W. Catalytic hydrogenation of 2,3,5-trimethylbenzoquinone over Pd nanoparticles confined in the cages of MIL-101(Cr). *Chem. Eng. J.* **2014**, *239*, 33–41. [[CrossRef](#)]
51. Thommes, M.; Kaneko, K.; Neimark, A.V.; Olivier, J.P.; Rodriguez-Reinoso, F.; Rouquerol, J.; Sing, K.S.W. Physisorption of gases, with special reference to the evaluation of surface area and pore size distribution (IUPAC Technical Report). *Pure Appl. Chem.* **2015**, *87*, 1051–1069. [[CrossRef](#)]
52. Khan, N.A.; Jun, J.W.; Jhung, S.H. Effect of Water Concentration and Acidity on the Synthesis of Porous Chromium Benzenedicarboxylates. *Eur. J. Inorg. Chem.* **2010**, *2010*, 1043–1048. [[CrossRef](#)]
53. Han, L.; Zhang, J.; Mao, Y.; Zhou, W.; Xu, W.; Sun, Y. Facile and Green Synthesis of MIL-53(Cr) and Its Excellent Adsorptive Desulfurization Performance. *Ind. Eng. Chem. Res.* **2019**, *58*, 15489–15496. [[CrossRef](#)]
54. Zhou, X.; Huang, W.; Liu, J.; Wang, H.; Li, Z. Quenched breathing effect, enhanced CO_2 uptake and improved CO_2/CH_4 selectivity of MIL-53(Cr)/graphene oxide composites. *Chem. Eng. Sci.* **2017**, *167*, 98–104. [[CrossRef](#)]
55. Aijaz, A.; Karkamkar, A.; Choi, Y.J.; Tsumori, N.; Ronnebro, E.; Autrey, T.; Shioyama, H.; Xu, Q. Immobilizing Highly Catalytically Active Pt Nanoparticles inside the Pores of Metal–Organic Framework: A Double Solvents Approach. *J. Am. Chem. Soc.* **2012**, *134*, 13926–13929. [[CrossRef](#)] [[PubMed](#)]
56. Swalus, C.; Jacquemin, M.; Poleunis, C.; Bertrand, P.; Ruiz, P. CO_2 methanation on Rh/ $\gamma\text{-Al}_2\text{O}_3$ catalyst at low temperature: “In situ” supply of hydrogen by Ni/activated carbon catalyst. *Appl. Catal. B Environ.* **2012**, *125*, 41–50. [[CrossRef](#)]